

Rietveld texture analysis from TOF neutron diffraction data

H.-R. Wenk^{a)}

University of California, Berkeley, California 94720

L. Lutterotti

University of Trento, Trento, Italy 38123

S. C. Vogel

Lujan Center, LANSCE, Los Alamos National Laboratory, Los Alamos, New Mexico 87545

(Received 24 February 2010; accepted 3 June 2010)

One of the advantages of a multidetector neutron time-of-flight diffractometer such as the high pressure preferred orientation diffractometer (HIPPO) at the Los Alamos Neutron Science Center is the capability to measure efficiently preferred orientation of bulk materials. A routine experimental method for measurements, both at ambient conditions, as well as high or low temperatures, has been established. However, only recently has the complex data analysis been streamlined to make it straightforward for a noninitiated user. Here, we describe the Rietveld texture analysis of HIPPO data with the computer code Materials Analysis Using Diffraction (MAUD) as a step-by-step procedure and illustrate it with a metamorphic quartz rock. Postprocessing of the results is described and neutron diffraction results are compared with electron backscatter diffraction measurements on the same sample. © 2010 International Centre for Diffraction Data. [DOI: 10.1154/1.3479004]

Key words: texture analysis, neutron diffraction, Rietveld method, quartzite

I. INTRODUCTION

The orientation of crystals in a polycrystalline aggregate (or texture) has a profound influence on physical properties, most importantly, anisotropy of bulk properties which are a function of anisotropic properties of single crystals and the orientation distribution. Texture has long been studied in metals as well as rocks [see Kocks *et al.* (2000) for details and applications] and we assume that the reader is familiar with the basic principles of texture analysis. Texture or crystallographic preferred orientation describes the orientation of crystallites of phases that compose a material relative to sample coordinates with a three-dimensional (3D) statistical orientation distribution function (ODF). The ODF can be calculated from measured pole figures of lattice planes (*hkl*). In the case of neutron TOF diffraction data the ODF is obtained directly as described below, but for representation we will use the more familiar pole figures, which have been calculated from the ODF. Textures are not only important for mechanical properties; they are also essential for crystal structure refinements and volume fraction estimates of aggregates with preferred orientation.

Various techniques are used to determine texture, most commonly X-ray, electron, and neutron diffraction (e.g., Wenk, 2006 and Wenk, 2011). Neutron diffraction has unique advantages for texture analysis because of high penetration combined with comparably large beam spot sizes. The information derived from the diffraction data is averaged over a large volume (typically in the order of a cubic centimeter); therefore, sampling statistically significant numbers of grains even in coarse-grained aggregates and special sample environments are possible. Time-of-flight (TOF) neutron diffraction is increasingly used to record textures of bulk

materials, providing the additional advantage of determining textures of low symmetry phases (e.g., Brown *et al.*, 2006; Xie *et al.*, 2003), of composites with complex diffraction patterns (e.g., Ivankina *et al.*, 2005; Wenk *et al.*, 2001), or *in situ* experiments at high/low temperature (e.g., Bhattacharyya *et al.*, 2006; Lonardelli *et al.*, 2007; McDaniel *et al.*, 2006; Wenk *et al.*, 2007) and stress (Hartig *et al.*, 2006). Since the Rietveld approach (Rietveld, 1969) is used to extract the texture information, it does not rely on single well-resolved diffraction peaks, as pole figure goniometers do, which are used for constant wavelength neutrons or X-rays. Neutron diffraction is most efficient with multidetector spectrometers such as high pressure preferred orientation (HIPPO) (at LANSCE, Los Alamos; Vogel *et al.*, 2004; Wenk *et al.*, 2003), GEM (at ISIS, U.K.; Day *et al.*, 2004), or SKAT (at the Joint Institute for Nuclear Research, Russia; Ullemeyer *et al.*, 1998), where each detector records a spectrum of crystals with lattice planes in reflection orientation.

It is not trivial to advance from diffraction spectra to quantitative orientation distributions. The Rietveld method (Rietveld, 1969), as implemented in the General Structure Analysis System (GSAS) (Larson and Von Dreele, 2004; Von Dreele, 1997) and MAUD (Lutterotti *et al.*, 1997), has proved to be a very powerful tool for texture analysis. Other Rietveld softwares such as FULLPROF (Rodríguez-Carvajal, 1993) or RIETAN-FP (Izumi and Momma, 2007) do not consider full texture analysis but merely offer corrections for preferred orientation and are thus limited to crystal aggregates with random orientation distributions or special cases such as orientation of plate-shaped crystallites in powders (Dollase, 1986). Here, we are not addressing methods or important applications of neutron diffraction texture analysis but focus specifically on the Rietveld method with MAUD, as applied to HIPPO data, providing an efficient hands-on procedure. Apart from data input with the MAUD wizard (described below), the procedure is equally applicable to any

^{a)} Author to whom correspondence should be addressed. Electronic mail: wenk@berkeley.edu

other TOF neutron diffraction data that are available in GSAS format. Also, the emphasis is on texture analysis, not on crystal structure refinement, microstructure, or residual stress.

MAUD is not restricted to neutron diffraction. It is used from two-dimensional (2D) X-ray diffraction images (e.g., Lonardelli *et al.*, 2005), microstructural investigations (e.g., Lutterotti *et al.*, 2004), and X-ray crystal structure analysis (e.g., Lutterotti and Bortolotti, 2005). Therefore, there are many options in MAUD that are not used for neutron diffraction texture analysis and this can make it overwhelming for beginners.

MAUD is not yet an established package like GSAS but constantly evolving, as new scientific applications require expansion and modifications. It is not a black box where you enter data and get results, and therefore it is not foolproof (no reference to FULLPROF!). For many applications there is no simple procedure and the user has to be familiar with many of the complexities. TOF neutron diffraction, one of the early MAUD applications (Lutterotti *et al.*, 1997), is an exception and here we want to guide a user with a step-by-step procedure through data analysis that is applicable to most routine samples, specifically for the LANSCE HIPPO diffractometer. Do not use this procedure for other applications such as texture analysis from synchrotron diffraction images. It is assumed that the reader is familiar with the general geometry of HIPPO (e.g., Wenk *et al.*, 2003). We will discuss a few of the many options that apply to neutron diffraction (especially in Sec. VI). MAUD is written in JAVA and works with any operating system for which a Java implementation is available (WINDOWS, MAC OS X, LINUX, and UNIX). For our demonstration we use WINDOWS XP. It should be noted that due to the complexity of the program and large data arrays, MAUD requires large memory (1 Gbyte is sufficient for most cases) and, while an analysis is running, users should refrain from running many other procedures at the same time, especially two simultaneous MAUD refinements.

We apply MAUD to determine the texture of a sample of amphibolite facies metamorphic quartzite from the Bergell Alps, measured in the HIPPO automatic sample changer Reiche and Vogel, 2010. The sample was roughly cylinder shaped with 1 cm diameter and 1.25 cm height (Figure 1). The data files as well as an instrument parameter file with information on instrument geometry can be downloaded from MAUD websites (<http://www.ing.unitn.it/~maud/tutorial.html> and <http://eps.berkeley.edu/~wenk/TexturePage/MAUD.htm>).

II. GETTING STARTED

When measuring textures, it is of critical importance to know the orientation of the sample relative to the diffraction instrument and thus the diffraction vectors relative to the sample for all spectra. Obviously, it is equally important to record and preserve the specimen orientation relative to the investigated larger scale object, e.g., a rolled plate or geological formation. Samples need to be oriented and then mounted in a systematic manner, for example, with an arrow pointing to a reference notch in a HIPPO sample holder (Figure 1). This yields the ODF and pole figures relative to the sample coordinate system such as the cylinder axis and the



Figure 1. Cylinder of rock, marked with an arrow to indicate orientation, mounted on a sample holder, with a characteristic notch.

arrow. Samples mounted on the sample holder's aluminum rod hang into the sample chamber with the aluminum shielded by neutron absorbing cadmium. If the latter is not applied properly, spurious peaks of aluminum would be observed and an additional phase might have to be added to the analysis.

For texture measurements with HIPPO, typically 720-³He-detector tubes, distributed over 30 detector panels and arranged on three banks (150, 90, and, 40° 2 θ), are used. Individual detector tubes of a detector panel are first corrected for variations in diffraction angle, then added (binned) at LANSCE, and finally exported in GSAS format (.gda files). For very coarse-grained samples with poor grain statistics it is advisable to inspect the raw binary data sets showing the histograms from each individual tube. This allows us to determine if the sample consists of only a few single grains and in such cases statistical texture analysis does not apply. The raw data are generally not distributed to users since the data sets are very large (>25 Mbytes per run). A software program to inspect those data sets is ISAW, which is available from the ORNL neutron portal at <http://neutrons.ornl.gov/portal/>. In addition to the binned data, the instrument scientist provides an instrument parameter file (.prm), obtained by measuring two standards (sample position and incident intensity), containing information about the geometry and calibration of the diffraction instrument.

The sample coordinate system in MAUD is defined by three right-handed cartesian, x , y , and z , and corresponding rotations, χ , ω , and ϕ , in that order [Figure 2(a)]. These rotations are the MAUD defined as positive for clockwise rotation (rotation axis pointing towards the viewer) and are the same as those of a standard texture goniometer, which means the rotation axes move when a rotation is applied. We will later explain how to apply a χ rotation of 90° to bring the HIPPO sample holder rotation axis into the center of the pole figure. After such a rotation around the neutron beam axis, the detectors plot on the pole figure as shown in Figure 2(b).

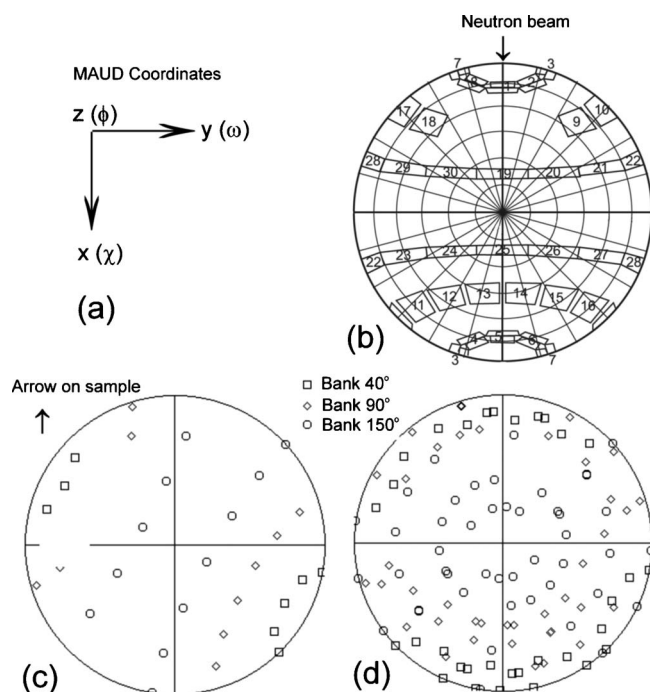


Figure 2. (a) Sample coordinate system in MAUD with three orthogonal axes and corresponding rotations χ , ω , and ϕ . (b) Pole figure coverage in the HIPPO TOF diffractometer. Neutron beam enters from the top. The area of each detector panel is displayed. Relative to Figure 2(a) the system has been rotated 90° around χ to bring the HIPPO rotation axis into the center of the pole figure. (c) Initial orientation in sample changer ($\omega=0^\circ$) with $\omega_{\text{offset}}=-61.7^\circ$. (d) four rotations to improve coverage. Equal area projection.

With the 30 detectors typically used for texture measurements, HIPPO has a large pole-figure coverage. Figure 2(b) displays the angular range that each detector panel views and thus the resolution that we can expect (Matthies *et al.*, 2005). In the data analysis we generally assume that detector data are representative of a point in the center of the polygon [Figure 2(c)]. Note that the coverage pattern of Figure 2(c) is rotated -61.7° around ω versus Figure 2(b). This is due to an offset of the rotation around the vertical axis introduced by the geometry of the HIPPO sample changer. Coverage can be improved by rotating the sample about the vertical axis into three or more different positions [Figure 2(d)]. Typical rotations in the sample changer, furnace, or cryostat are $\omega=0^\circ$, 4° , 67.5° , and 90° . Positive numbers assume that rotations are counterclockwise.

Each measurement of a given orientation with HIPPO takes between 1 and 60 min, depending on the volume and complexity of the sample. Thus, with four rotations, a measurement is done in less than 1 h for most samples. With the automatic sample changer up to 16 samples can be measured automatically, without operator interaction.

III. ENTERING DATA

1. Download the latest version of MAUD from the web (<http://www.ing.unitn.it/~maud/>) and install it on your computer in a separate directory. Be aware that MAUD is being updated periodically. You also need a recent version of JAVA (version 6 or higher is preferred:

Figure 3. HIPPO Wizard in MAUD to load instrument parameter file and data files.

java.sun.com/javase/downloads/index.jsp). JAVA is not installed by default in the WINDOWS operating system and the open source JAVA implementation preinstalled on most LINUX distributions (e.g., UBUNTU) at present is not suitable to run MAUD (install the last SUN version from the previous link). Also, download the HIPPO demo data set into your computer and store it in a separate directory. Then start MAUD. If you start MAUD for the first time it will ask you to accept the license and where to store additional files. It is most convenient to have those in the MAUD directory. The MAUD console window will output information during the operation that can be useful to identify problems.

2. The menu option "File→New→Hippo Wizard" opens a window [Figure 3] that allows you to conveniently import the experimental data and prepare them for the automatic analysis.
3. In the Hippo Wizard window, input a title describing the data set.
4. Select the parameter file that corresponds to your data by clicking on the "Browse" button next to the "Choose calibration file" field (for this demonstration we use `hippo_sc_050819_30panel.prm` from the demo data). After defining the instrument parameter file, select data files with the second browse button (for example, `14445.gda` to `14448.gda`).
5. Assign each data file a rotation angle omega (for the test sample: 0° for `14445.gda`; 45° for `14446.gda`; 67.5° for `14447.gda`; and 90° for `14448.gda`). The bulk rotation, "Omega offset" (-61.7°), accounts for the HIPPO sample changer oddity that the sample holder notch is displaced from the incident beam direction at 0° rotation angle. Applying this rotation realigns the sample, with the arrow pointing to the top in the reconstructed pole figures. Click on each file again to verify that the angles were assigned correctly.
6. Click "Next" and choose the d ranges to be considered for each detector bank. This range depends on the number of peaks in your patterns. For instance, if the maximum reflection d spacing is at 2.3 \AA , choose a maximum d spac-

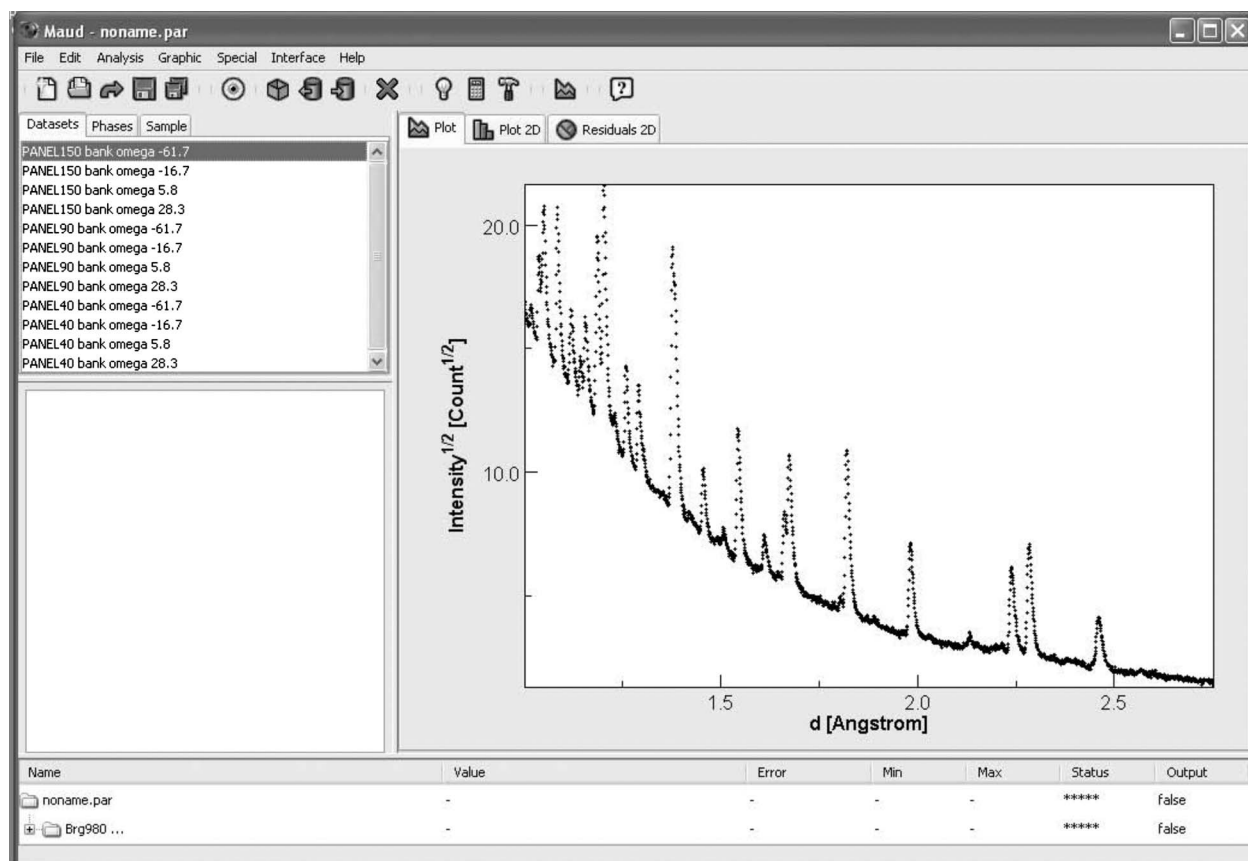


Figure 4. Main MAUD page with Plot display for 150° detectors: enter the data sets and disable faulty spectra.

- ing of 2.5 Å since all data above this upper limit represent only background. For this example, we use 1 to 2.75 Å. Data at lower d spacings do not improve the analysis (in this case) because of the large number of overlaps. Restricting the range also speeds up the computation. Generally, you consider each bank and each rotation as a different instrument and refine instrumental parameters accordingly—namely, the scaling factors and conversion factors for TOF to d spacing (DIFC). Hence, leave the corresponding option in the dialog checked.
7. “Finish” the Wizard. This returns you to the main MAUD page. Data are displayed either as average profile (Plot tab panel on the right hand side of the main window) (Figure 4) or as a stack of all spectra for a given “Instrument” (Plot2D tab panel) (Figure 5). There are various options for graphic displays: they can be selected in the main menu “Graphic→Plot options” or in “Analysis→Preferences.” For this presentation we use black and white representation. For Plot this is in “Preferences” under the “plot.black&white” key “true” and for Plot2D in “Preferences” under the “Multiplot2D.grayscale” key “true” (Preferences are in alphabetical order, first upper case, then lower case). In the menu “Graphic→Plot options” we choose “sqrt” for intensity scale (log 10 scales are used mainly for reflectivity analysis plotting). There are various options for X scale, 2θ , d spacing, or Q , depending on the application. Background can be subtracted or plotted separately (in Figures 4 and 5 we do not subtract background). Spectra can be displayed normalized with the incident spectrum (“Calibration correction,” as

defined in the instrument parameter file); the refinement, however, uses actual intensities. We can also select font and font size.

8. You may now inspect your data using the “Plot2D” panel and by clicking on each “Dataset.” Note the bottom (first) spectrum of the 90° bank detectors has a much lower intensity (Figure 5) due to partial shielding of tubes by the sample changer and we may want to remove it from the analysis. Edit the data set in the “Datasets” panel (“Edit–Edit Object” or the “eye” shortcut in the middle of the toolbar, just under “Special”). On the window that opens there is a variety of information about your data (Figure 6). Editing “Diffraction Instrument” (press the “Edit” button in the instrument panel) displays details about the experimental setup. In the case of TOF neutron diffraction, the HIPPO Wizard has already initialized all important information (subwindow in Figure 6). For other TOF diffractometers you may have to modify some entries. On the main window (Figure 6) you may modify the computation range or you can exclude some regions from the spectrum. The units are d spacings for TOF neutron diffraction (converted from TOF in the .gda file), 2θ for angular dispersive experiments, and energy for energy dispersive experiments. Choosing “Datafiles” opens a window with the individual diffraction spectra, including orientation angles (Figure 7). The orientation angles are initialized for HIPPO data by the HIPPO wizard. For other instruments or other rotations in HIPPO, e.g. around a horizontal axis instead of the vertical axis, the proper sample orientation angles need to be entered here. The

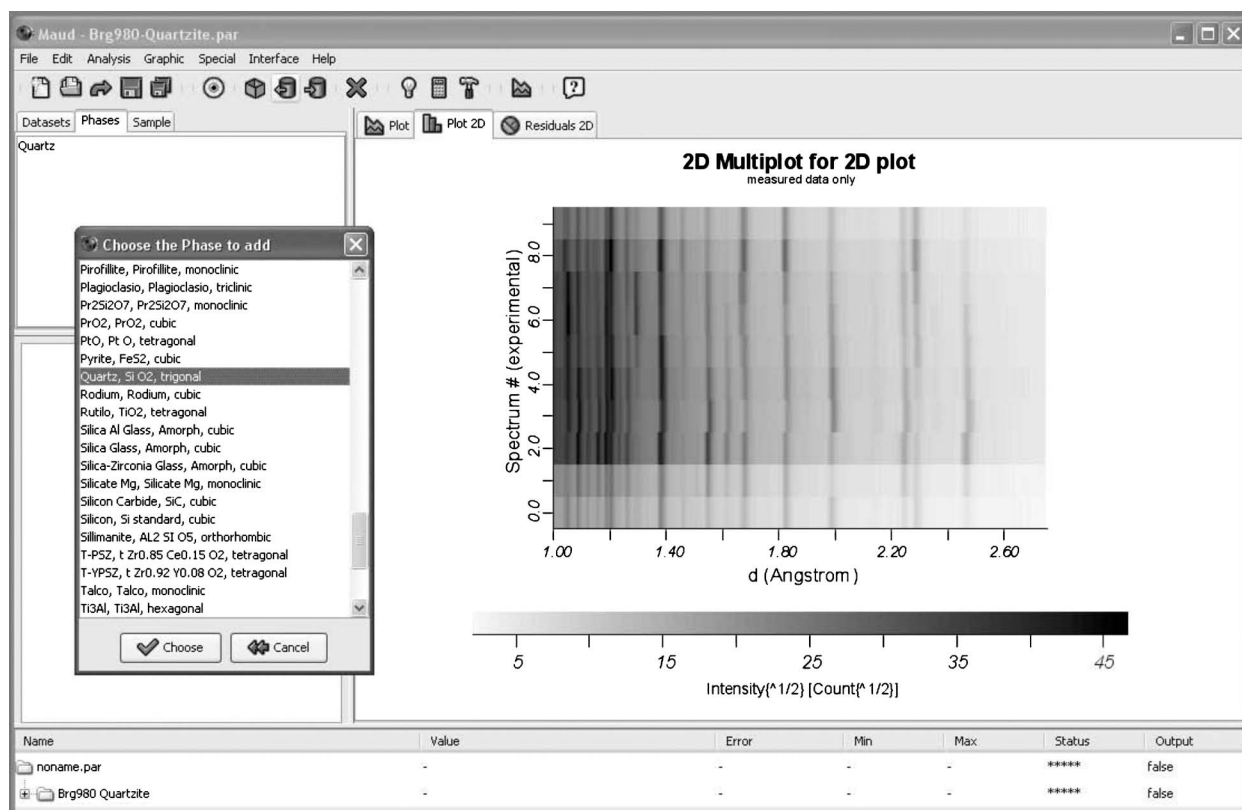


Figure 5. Main MAUD page with Plot2D display for 90° detectors: disable faulty spectra, such as the one at bottom (No. 9), then enter phases (the database “structures.mdb” window is shown) and edit the sample.

angle η defines the azimuth angle of HIPPO detectors around the incident beam for a given Bragg angle. To exclude the first spectrum [14445.gda (9)], disable the first spectrum on the list (No. 9) for all four 90° banks. (Select the spectrum and click on the “Enabled” check button to disable. By default each data set and datafile in the data set is enabled.)

- Next, click on the “Phases” tab and load phases. This can either be done from a cif file which you have downloaded from a database [such as the free COD database, containing more than 100'000 phases at present, <http://www.crystallography.net/>, Grazulis *et al.* (2009), or the equally free Mineralogical Society of America database <http://rruff.geo.arizona.edu/AMS/amcsd.php>, Downs and Wallace-Hall, 2003] or access structures coming with the MAUD installation in the file structures.mdb. Select from the principal menu “Edit” and “Load phases from CIF data base or file...” or click the left arrow icon in the toolbar. You can create your own version of the structures.mdb file by exporting crystal information in MAUD to it for further use (right arrow icon in the toolbar). You can also enter your own crystal structure information (space group, lattice parameters, atomic coordinates, etc.) using the “Add new object” in the menu for the “Phases” tab and then the “Edit object” command. For this example, use “Quartz” from the MAUD database (Figure 5). Looking at the structure data (with “Edit object”), we see that temperature factors $B(=8\pi^2 U_{iso})$ for Si and O are zero. The reason is that the cif file contains anisotropic temperature factors which are currently not loaded in MAUD from cif files. Zero is not realistic and we enter

“1.0” for each instead. We will later refine the temperature factor but keep it the same for all atoms. Temperature factors generally vary between 0.2 and 1.5 for most atoms and crystal structures at ambient temperature. Also, note that if we use the HIPPO wizard, automatically neutron scattering lengths for natural isotope abundances of elements are applied. In case other isotopes are required, they can be specified in the “Edit object” window under the tab “Structure” by pressing on the button to select the element type. In case more than one isotope is present and not in natural abundances, enter each isotope as a separate atom site with corresponding occupancies. If multiple phases are present, repeat this step for each phase.

- Edit each phase, and in the “Advanced Models” tab check that “Le Bail” is the actual “Structure Factor Extractor” (this is the default for the HIPPO wizard), then choose E-WIMV as a texture method. Under the texture options (press the “Options” button for the texture method), select an ODF resolution between 7.5° and 15°, which approximates the angular resolution of HIPPO [Figure 2(b)]. Here, we use 15°. You can also impose sample symmetry after you verify that the data warrant it and your sample is properly oriented; i.e., the symmetry axis of a fiber symmetric texture is in the center of the pole figures (no symmetry is imposed here). You can use the “Sample position” window (under “Sample window” to reorient the sample with respect to laboratory coordinates to ensure correct symmetry. Under “E-WIMV Advanced Options” you can restrict the number of reflections that are used in the texture refinement either by intensity or by d spacing (we use defaults

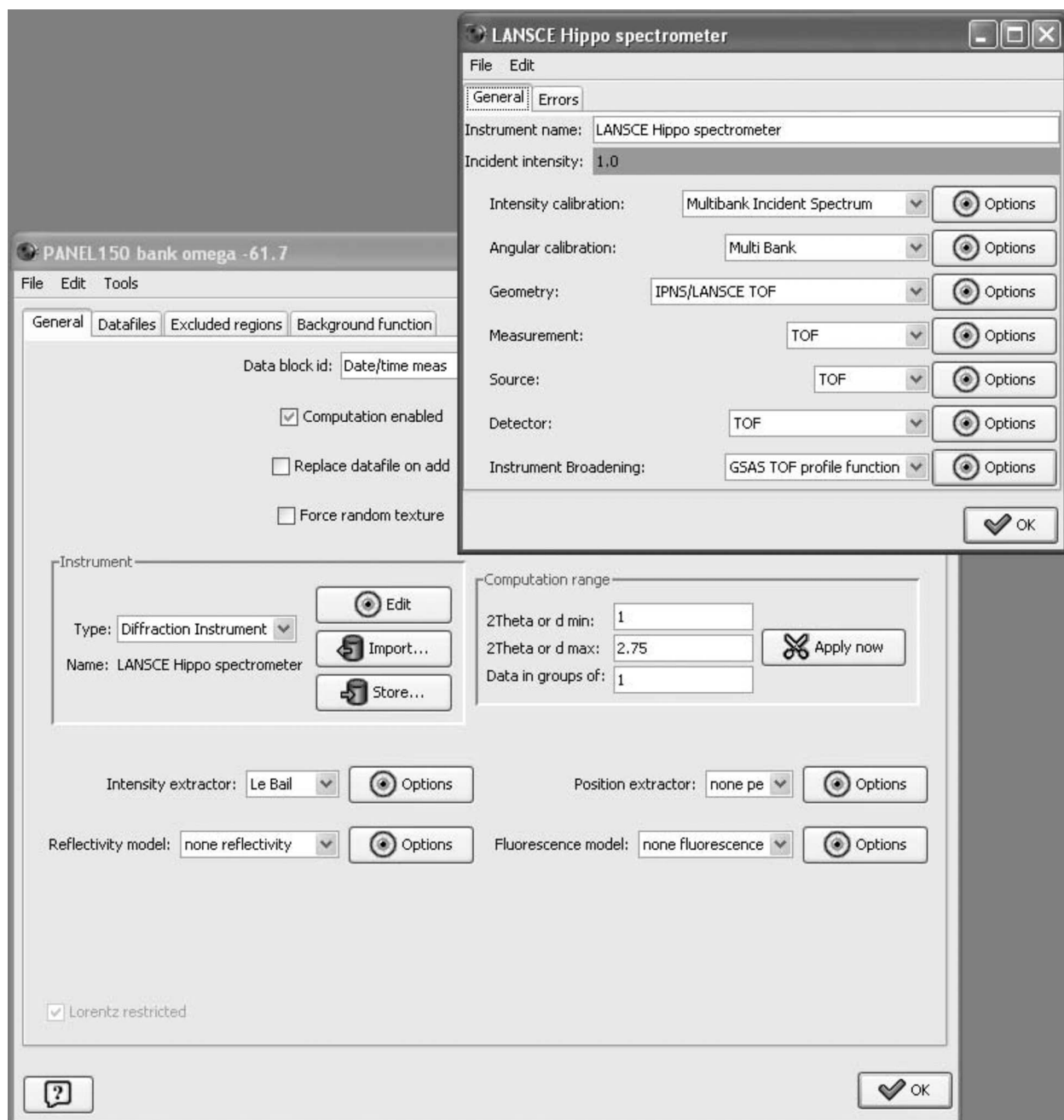


Figure 6. Data set window with options to edit “Diffraction Instrument” (Window for HIPPO parameters is inserted), Datafiles, Excluded regions, and Backgrounds, as well as changing Computation range.

0., 0.). (On the main window, in “Analysis-Options” make sure to “Enable texture extraction” at “end of iteration” which is the default).

11. If you need the sample rotation axis in the center of the pole figure, edit the “Sample” and under “Sample position” choose $\chi = -90^\circ$. This orients the system such that the sample changer rotation axis is perpendicular to the plane of the pole figure. In the final pole figure (Figure 10) you are looking down on the sample hanging in HIPPO, with the face of the sample glued to the holder facing the viewer and the arrow pointing to the notch located at 12 o’clock. To obtain pole figures viewing the sample standing on the holder as shown in Figure 1 and the arrow pointing to the notch at 6 o’clock (the conven-

tional setting), the sample position angles need to be set to $\chi = -90^\circ$ and $\varphi = -180^\circ$. You can verify the relation between instrument and pole figure coordinate system by plotting the pole figure coverage at any time (in “Graphic-Texture plot”)—the 90° detectors have a characteristic gap for the HIPPO door, which allows us to identify the direction of the incident beam. The implementation of the E-WIMV algorithm in MAUD (see below) requires that for strong textures [pole densities > 10 multiples of a random distribution (m.r.d.)], the strongest pole figure maxima to be preferably near the center of the pole figure, otherwise the differences in sampling density may result in artifacts. If a strong texture is observed after the first analysis with the strongest

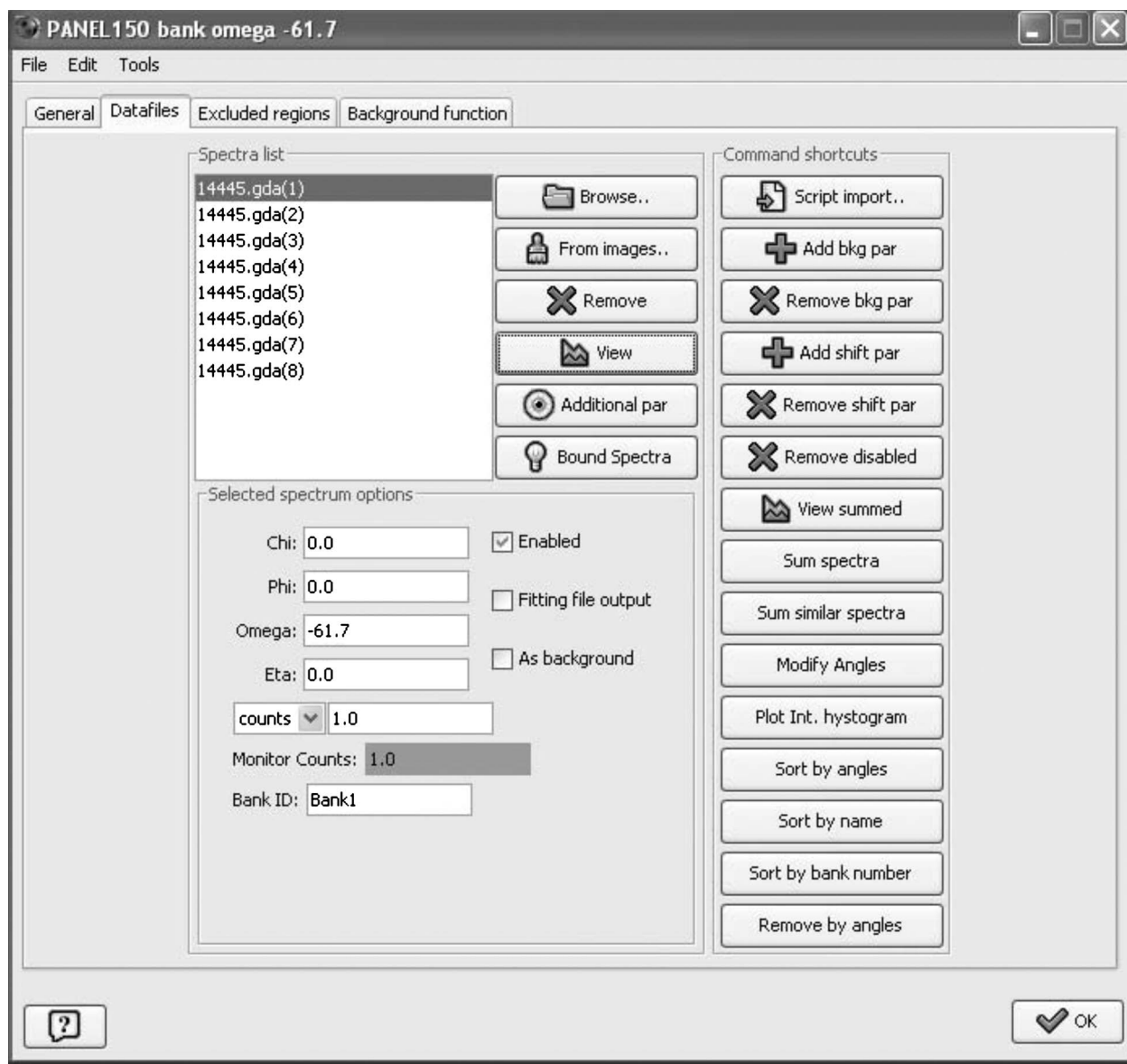


Figure 7. Datafiles window which can be used to disable certain spectra.

maxima on the rim of the pole figure, reorient the sample accordingly in the “Sample” tab. Three rotations around orthogonal axes are shown in Figure 2(a). The first rotation is ω , second is χ , and last one is ϕ ; all rotations are clockwise. For polyphase materials you can enter initial estimates of the volume fractions in the “Layers” dialog of the “Sample” tab (default is equal weight fractions for each contributing phase). These volume fractions will later be refined.

12. At this point, you should save your analysis in your data directory (from main menu: “File→Save analysis as”) as a “.par” file (we use Brg980-Quartzite.par). Save the analysis after each successful refinement cycle. Then you may re-load the file later and choose “Analysis-Compute Spectra” to re-initialize the values, e.g. for texture plotting, without the need of a full analysis. Now you are ready to start the refinement.

IV. RIETVELD REFINEMENT

During the least-squares refinement you may look at parameters, e.g., lattice parameters, on the parameter list panel on the bottom of the main window. You can also view them in “Phase” by selecting the corresponding phase object to find the cell parameters. It is advised not to open the “Edit phase” window during refinement. This may interfere with the least-squares routine if you modify something. Even if you modify nothing, it is important to close these frames using the button on top of the window (on WINDOWS XP the small button with an “X” in the title bar on the top right of the window) and not using the “OK” button. The latter changes or refreshes the parameters in midst of the refinement and may cause the optimization routine to compute wrong quantities and behave erratically.

For simple analyses/materials you can use an automated procedure (and this is the case for our example). Under the

menu “Analysis” select “Wizard.” In the appearing window choose “Texture Analysis” in the right panel and press the button “Go!” You may watch the progress of the refinement in the graphics window (Figures 4 and 5). The automatic procedure with the Wizard will refine the most important parameters in four cycles. Select no more than five iterations (this can be adjusted as the refinement proceeds with the proper indexed scroll bar in the iteration output panel of the main window). To guarantee convergence, you may, at the end, perform three to five additional iterations (selecting from the menu “Analysis→Refinement”).

The texture wizard works well for single-phase materials and clearly defined compounds with a light/medium texture. For complex materials you need to proceed in individual steps using the menu “Analysis→Parameter List” and specify manually the parameters to refine. You can also initially use the wizard to set up automatically the parameters and adjust them later. To do this, in the wizard select the cycle step you want to perform (left panel) and press the “Set parameters” button instead of “Go!” Then open the parameter list window to manually select the parameters to be refined. The parameter list is also displayed at the bottom of the main window and by setting the “Status” of an individual parameter to “Refined” it is allowed to vary. Using the “Equal to” option constraints between parameters may be introduced (e.g. atomic positions of atoms on shared sites are forced to remain the same).

If you do everything manually you may proceed as follows: fix all parameters first (using the corresponding button “Analysis→Parameter List”), then free backgrounds and scale parameters (with corresponding buttons), and then close the parameter list window and perform a refinement (“Analysis→Refine” in the main menu). Next, add to the refinement “Spectra Monitors→TOF Bank SF” (with the buttons in the parameter list window) and finally “Texture,” depending on how the procedure converges. Section VI will discuss some of the options.

Be aware that the least-squares procedure refines many parameters (over 1000 in many cases). Most parameters are complex nonlinear functions and the total model used to describe the experimental data and deviations from these data is a surface with many subsidiary minima. If too many parameters are refined from unrealistic starting positions, then the refinement may converge into subsidiary minima rather than the true solution or lead to divergence. It is therefore important to have starting parameters as close as possible to the true solution. If necessary, parameters can be adjusted manually. Use “Datasets”→“Datafiles”, select a spectrum and “View.” With “Tools”→“Change parameter” you can change parameters manually and immediately see the result.

Below we only consider the “Texture Wizard.” The cycles for the automatic refinement of the texture are the following:

Cycle 1: Refining the scale factors, background parameters, and phase fractions for multiphase systems. The calibrated incident intensity parameters (12 parameters) are directly loaded from the HIPPO calibration file and then kept constant. A single scale factor is refined for each detector panel, accounting for differences in detector efficiency or varying attenuation along the path between sample and detector. Backgrounds are expressed with a polynomial. Three

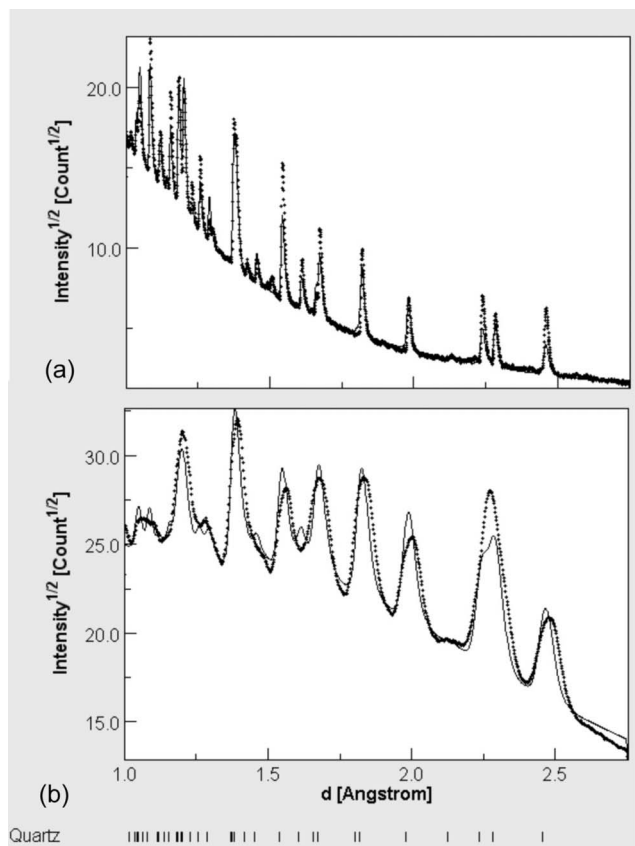


Figure 8. The fitting of scale factors and backgrounds for (a) 150° and (b) 40° bank average spectra (cycle 1). Note the much higher angular resolution of the high-angle detector, but poorer counting statistics. Spectra are not normalized.

background coefficients are refined for each bank (by default only three background coefficients but more can be added) and, in addition, two background coefficients for each pattern (view in “Datasets—Datafiles—Additional parameters”). After the cycle, the background starts to look reasonable and so does the overall intensity (Figure 8). Note that the high-angle 150° bank detectors [Figure 8(a)] have a much higher resolution, i.e., narrower peaks, than the 40° bank [Figure 8(b)], but lower counting statistics, i.e., noisier data. Texture is not yet reflected in the recalculated spectra [top of Figure 9(a)]. Also, the wavy line is not matched due to mispositioning of the sample, which is particularly serious for the 40° bank.

Cycle 2: In addition to the previous parameters, peak positions are adjusted during this cycle by refining cell parameters and the conversion parameters for TOF to d spacing conversion based on observed d spacings. This essentially corrects for sample alignment problems which may originate even from changes in position of the center of gravity of the scattering power relative to the calibration material due to changes in the scattering power of the material. The waviness is corrected [Figure 9(b)].

Cycle 3: The microstructural parameters (crystallite size and microstrains) are added to the refinement to adjust peak shapes. There are several methods to refine crystallite size and lattice strain (see also Sec. VI). In this example we use a simple isotropic model, which is the default. Only one overall temperature factor, B , is used for all atoms of all phases to

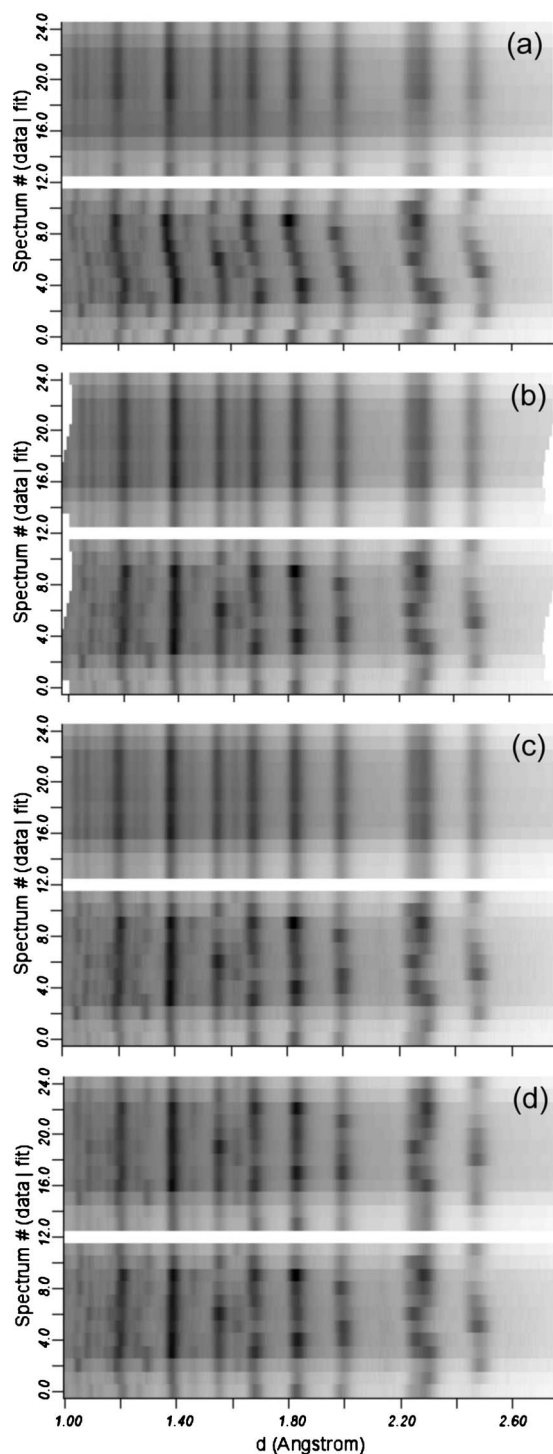


Figure 9. Texture Wizard with multiplots illustrating refinement stages in (a) cycle 1, (b) cycle 2, and (c) cycle 4 for 40° detectors of -16.7 rotation. Top calculated; bottom observed.

avoid correlations and minimize possible errors. Other structural parameters, such as atomic coordinates, are not refined with the texture wizard. You may refine them separately at the end, including individual isotropic temperature factors, but this requires excellent resolution and counting statistics.

Cycle 4: The orientation distribution is refined with the chosen texture extraction method, in our example the E-WIMV algorithm (Matthies and Vinel, 1982; more options are briefly discussed in Sec. VI). Intensities of individual

peaks start to match [Figure 9(c)]. Warning: the interactive Plot2D display only shows the real calculated pattern at the end of each cycle. In between it may indicate a perfect match, but this is due to temporary fitting by the Le Bail extraction, not true texture intensities.

The procedure with the Wizard does not automatically refine all possible parameters for all phases. For example, crystallite size and microstrains are not refined for phases that are below a certain threshold. The default threshold (0.001) can be changed in “Analysis→Preferences” “wizard.riet_refine_sizestrain_over” key.

After this refinement, several checks need to be performed. The overall quality of the least-squares refinement is expressed in R or R_{wp} factors, with 5% to 15% for a good fit. These numbers are also included in the file generated by “Analysis→Results.” There are separate R factors for texture and overall refinement because the WIMV and E-WIMV methods use their own algorithms to fit the experimental texture data extracted with the modified Le Bail procedure (Matthies *et al.*, 1997). However, R factors are only a bulk measure (e.g., Toby, 2006) and do not provide details about potential problems. Refining more parameters may provide a better fit (lower R factors) but adding parameters is only justified if these parameters are constrained by the actual data. The best evaluation of a satisfactory refinement is to compare observed (bottom) and calculated (top) intensities for all detectors on the multiplots [“Plot2D,” Figure 9(c)]. In the “Datasets” editing window under “Datafiles” select the spectra, one or more at a time, and press the “View” button to get a closer look at observed and calculated intensity spectra. The “Plot” panel on the main window can be misleading for evaluating the fit. It is a simple average over all spectra for a data set and does not take complex texture relationships into account.

If the results appear reasonable, close all windows, except the main window, then select “Graphic→Texture Plot” to display the checked pole figures (Figure 10). “Reconstructed intensity” shows pole figures of selected lattice planes hkl calculated from the ODF. “Experimental intensity” displays normalized Le Bail factors. In this window you can also confirm that you have the correct “Pole figure coverage” [Figure 2(d)]. Particularly for texture publications we generally prefer gray shades for density mapping (click “Gray shaded” on “Texture plotting” page). Colors may be more glamorous for presentations, but, if colored pole figures are copied on a black-white printer, the pole densities become unintelligible, with both minima and maxima appearing dark. More details about texture representation are given in Sec. VI.

The Wizard refinement is often sufficient to capture the main texture features. You may wish to continue to refine additional parameters from the many possibilities offered by MAUD. They include lattice parameters for accessory phases, atomic coordinates, temperature factors, anisotropic grain size, and residual stresses. This can be done in “Analysis→Parameter List,” fixing the ones you do not want to refine and refining those you do by selecting them in the list and changing their status to “Refinable.” Otherwise, you can edit the individual parameters in the individual edit windows (for phases, data sets, instruments, and sample), and select them to refine (by pressing the right mouse button when over any

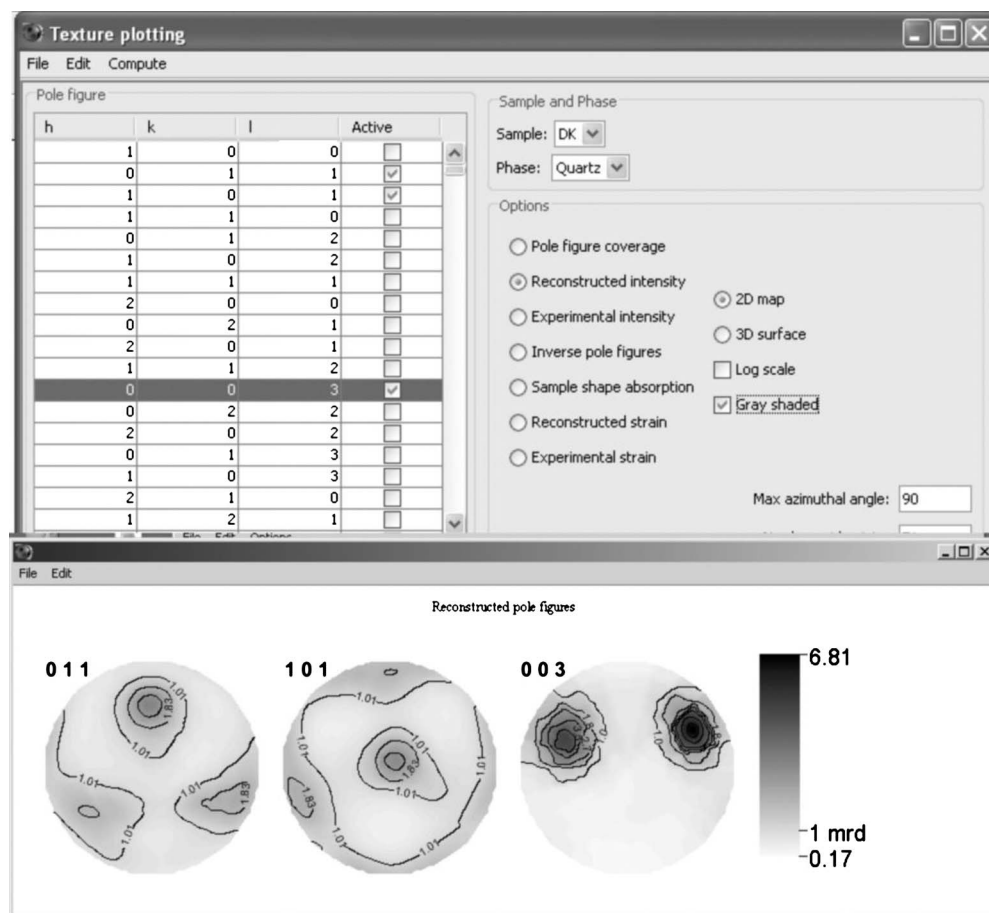


Figure 10. Texture plot window and selected 011, 101, and 003 pole figures to plot. The actual plot of pole figures (reconstructed intensity) is shown at the bottom.

of the parameter text fields). Be aware that the refinement is limited by the quality of the data. For TOF neutron diffraction there is some inherent uncertainty about the sample position and correspondingly absolute lattice parameter values. Also, for HIPPO peak resolution, even for 150° detectors, is not extreme and thus information, e.g., on residual strain may not be possible to extract.

V. EXPORTING TEXTURE DATA

For further processing of the texture data, the ODF can be exported as an ASCII file (in the E-WIMV options window) in BEARTEX format (.mod) (Wenk *et al.*, 1998). ODF densities in m.r.d. are interpolated for 5° × 5° cells. Then, in BEARTEX (<http://eps.berkeley.edu/~wenk/TexturePage/beartex.htm>) the MAUD format is first converted to the standard binary format in routine CMAU. Subsequently, it is smoothed to alleviate the rigid cell structure by applying a 7.5° Gauss filter (SMOO). With this smoothed ODF you can then calculate pole figures (PCAL) and plot them as shown in Figure 11(a) (PING) in a format that is preferred for publications. From the continuous ODF weighted individual orientations can be generated for use in polycrystal plasticity simulations (ODFW). Also, you can use this ODF to calculate polycrystal physical properties (TENS). In CSEC you can rotate the sample coordinate system.

As a comparison, we analyzed the same quartzite sample with the scanning electron microscope using the electron back-scattered diffraction (EBSD) method. For EBSD, 5824 orientations were used, then smoothing the ODF with a 15° filter and rotating the EBSD-ODF to get it into the same orientation as the neutron pole figures [Figure 8(b)]. The two sets of pole figures are similar, including pole densities, but EBSD data that rely on much smaller numbers of grains show stochastic effects and are statistically less relevant (Matthies and Wagner, 1996; Matthies *et al.*, 2005), underlining the main advantage of neutron texture analysis.

An interesting feature of this quartz texture is that 101 poles align perpendicular to the schistosity (center of the pole figure). Mechanical twinning causes this feature and the pattern can be used as a paleopiezometer to unravel the stress history (Wenk *et al.*, 2006). Also, in the resolution of positive (101) and negative rhombs (011), which are required for such analysis, neutron diffraction excels over EBSD. With EBSD some of the pseudohexagonal orientations that define the trigonal symmetry may be misindexed.

VI. DISCUSSION OF SOME OPTIONS

In this section we are discussing some options for advanced MAUD users.

(a) We have already mentioned the “Preferences” ASCII file.

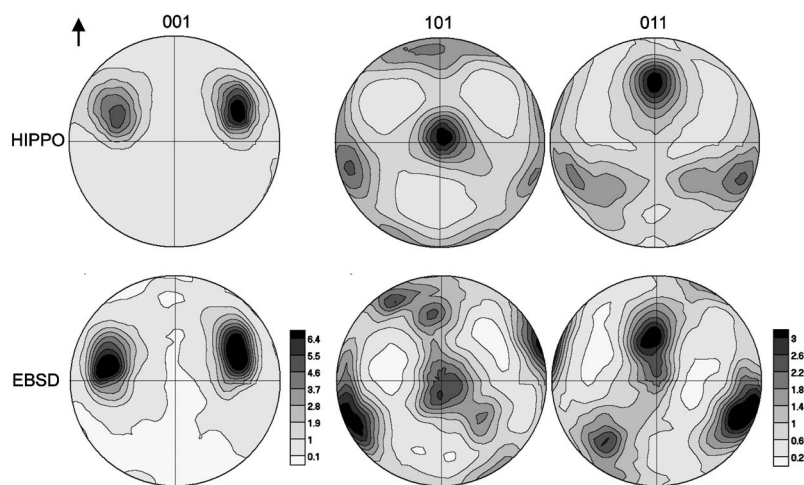


Figure 11. Pole figures of c axes (001) and positive (101) and negative rhombs (011) of trigonal quartz, recalculated from the ODF and plotted with BEARTEX for publication quality. HIPPO data (top) and EBSD data (bottom) for the same sample. Equal area projection, upper hemisphere.

Defaults are generally appropriate but occasionally you may want to change them. The “Preferences.Maud” file is stored in the MAUD directory and any changes will be applied permanently. Below are some keys for preferences that you might want to change:

- Multiplot2D.grayscale* (default is false): controls the 2D plotting in colors or B/W
- log_output.fullResults* (default is false): generate long or short listing log output
- plotExpPF.minimumDistanceDeg* (default is 10): in the experimental pole figure plot, control how far from measured point the interpolation goes
- wizard.riet_remove_phases_under* (default is 0.01): remove automatically phases from refinements when below 1% volume fraction (these are set to zero).

(b) *Where are the results?* Results (with standard deviations) are stored in the parameter list (on main MAUD page). They are also contained in the ASCII file “Results” with information about the refinement as well as a reflection list with intensity, size and strain information, and texture. This file is written as a “lst” file in the directory of parameter and data files. For E-WIMV the “lst” file contains normalized pole densities for all ODF cells in gamma sections.

Parameters, including errors, can also be exported as an ASCII file that can later be processed by EXCEL, etc. In “File,” choose “Append Simple Results to...” or “Append Results to...” For “Append Simple Results” first create an empty text file in your data directory. For “Append Results” you also need to create a text file, but in this case it will only write parameters for which, in the parameter list, the option for “Output” has been set to “true.” By default all are set to “false.”

(c) *Background options.* Two types of background are refined. One is for each detector and one for each spectrum. For the detector background there are various options. Often a polynomial is used. It is not advisable to use more than four coefficients (default with the HIPPO wizard is 3). Alternatively backgrounds can be interpolated between manually set values or points chosen automatically by the routine [using the method described by Sonneveld and Visser (1975) in Sec. III]. MAUD does not interpolate the background on the

experimental pattern, but to avoid using peak intensities as background, it computes the interpolation on the experimental pattern after subtraction of the intensities due to phase reflections. This way the choice of the points becomes less important. Background functions for each spectrum are added in “Datafiles → Additional parameter” and two coefficients are generally sufficient. In most cases the defaults of the HIPPO wizard are adequate and the user does not have to worry about it. For interpolated backgrounds there is a specific tab panel next to the one for the polynomial general background in the data set editing window. Manual points can be chosen graphically in the plot.

(d) *Texture models.* There are various texture models implemented in MAUD (“Phases → Advanced Models → Texture”). This is not the place to discuss texture analysis in detail and we refer to standard texts (e.g., Kocks *et al.*, 2000; Matthies *et al.*, 2005). Some methods are in direct space (WIMV, E-WIMV, and ideal components). There is also the option to use the harmonic method which works in Fourier space. For most applications the E-WIMV method is preferred. The main options are the cell size (generally between 5 and 15) and sample symmetry. However, sample symmetry should only be imposed after it has been verified that it statistically exists and the sample has been properly oriented (fiber symmetry around center of pole figures, orthorhombic symmetry with horizontal and vertical symmetry axes, etc.). The cell size depends to some extent on the pole figure coverage by data. In order to provide a solution, each ODF cell must be covered by at least one data point (and preferably more), i.e., the coverage must be 100%. On the E-WIMV option panel the ODF hits can be viewed (at least one hit per cell) as well as ODF weights which are interpolated, taking neighboring cells into account. If the coverage is less than 100%, either the cell size must be increased or more data need to be added (e.g., larger d range) or a method such as harmonic or ideal components must be applied. The texture refinement relies on the Le Bail factors (Le Bail *et al.*, 1988), i.e., the fraction of the experimental intensity and the structure factor with no texture present. In the “E-WIMV → Advanced Options” panel weak reflections can be excluded from the texture calculation. This is useful to avoid artifacts.

(e) *Texture representation.* All texture analyses rely on the

ODF which is a 3D function describing the crystal orientation frequency of crystallite orientations represented in sample coordinates. The latter is done with the Euler angles and there are various conventions such as ϕ_1, Φ, ϕ_2 (Bunge, 1965), Φ, Θ, Ψ (Roe, 1965) with $\Psi = \phi_1 - 90^\circ$, $\Theta = \Phi$, and $\Phi = \phi_2 + 90^\circ$. MAUD uses the formulation α, β , and γ of Matthies and Vinel (1982) that is identical to Roe. The overall texture strength can be evaluated with the Texture Index F2 (Bunge, 1982), but a more satisfactory representation is the 3D ODF which can be viewed in rectangular coordinates or in less distorted cylindrical coordinates (Wenk and Kocks, 1987). Often textures are represented as pole figures [in sample coordinates for one crystal lattice plane normal (hkl) or symmetrically equivalent sets $\{hkl\}$] or inverse pole figures (in crystal coordinates for one sample direction) which are 2D projections of the ODF. These graphic representations are available in “Graphic→Texture plot” and there are various options. Note that all pole densities (ODFs as well as pole figures) are normalized to express densities as m.r.d. The “Texture plotting” routine allows us to plot ODFs, pole figure coverage, reconstructed pole figures, and experimental intensity [in “Preferences” “plotExpPF.minimumDistanceDeg,” the range of interpolation can be set (default is 10)]. The pole figure coordinate system depends on how the sample has been mounted in the diffractometer and how “Sample position” has been set. For inverse pole figures [001] is in the center and the pole to (100) to the right. Three inverse pole figures are plotted for normal direction (ND), rolling direction (RD), and transverse direction (TD). ND is normal to the pole figure [z in Figure 2(a)], RD is pointing vertically [x in Figure 2(a)], and TD horizontally [y in Figure 2(a)]. Often ODFs and pole figures are exported as ASCII files for further processing in other programs.

(f) *Line broadening* is convoluted by two terms: instrument and sample broadenings. The first one depends on instrument setup (only slightly on sample dimension and transparency) and can be kept constant as it was determined during the instrument calibration. Instead the second part of the broadening can be different for each phase and in MAUD is the only broadening that should be refined during an analysis. This simplifies the refinement for the HIPPO user, as he will only refine two parameters (crystallites and microstrain mean value) for each phase instead of refining all Caglioti parameters for each phase (Caglioti *et al.*, 1958; Caglioti *et al.*, 1960). The instrument broadening is described by the formula for the TOF profile function as described in the GSAS manual (Larson and Von Dreele, 2004) and is loaded directly with the instrument parameter file.

For the microstructural broadening there are different options available in MAUD. The default model uses two parameters (mean crystallites and microstrain “Delft” method) for isotropic broadening [Eqs. 6 and 7 of Lutterotti and Scardi (1990)]. If one phase exhibits anisotropic broadening the method of Popa (1998) can be selected where the crystallite and microstrain anisotropy is described by a harmonic expansion and the crystallographic symmetries are imposed through the Laue group of the phase. The best fit with the smaller expansion should be pursued. Another model for anisotropic broadening is the “anisotropic–no rules.” The method is described by Lutterotti and Scardi (1992). In this model crystallographic symmetries should be imposed simi-

larly to what is done for anisotropic temperature factors using the point symmetry. The last model available can use both the isotropic or anisotropic model but instead define a different way to compute the peak profile and to convolute crystallite and microstrain effects. It is called “distributions” and instead of a defined profile function it computes the peak shape from Fourier transforms of the convoluted crystallites and microstrain distributions. The crystallite distributions employed are described by Popa and Balzar (2002) and the microstrain distribution was used by Lutterotti and Scardi (1992). It is composed of two terms: a mean microstrain and a “slope” coefficient to account for dislocations or defects distributed inside the grain or at the grain boundary.

When revising the results for anisotropic broadening, in general do not rely on 3D grain shape representation (when available) but rather on the size in different lattice directions hkl (under “Results”). For microstrain refinement, a medium large d range is required. MAUD can be used to refine structural features of amorphous materials as described by Lutterotti *et al.* (1998). For planar defects additional models can be selected from the Warren description of planar faulting to a single layer model for turbostratic disorder (Lutterotti *et al.*, 2010).

Be aware that neutron diffraction data may not have sufficient resolution to refine rms microstrain and particle size and generally no attempt should be made to refine those parameters, even if R factors improve.

(g) *Absorption*. One of the advantages of neutrons is that for most materials there is excellent penetration and absorption is minimal. However, there are cases where absorption needs to be considered, e.g., in the analysis of texture in silver coins with a very high neutron absorption (Xie *et al.*, 2004). The shape can be entered in “Sample” “Sample Dimensions” “Shape model.” The “Harmonic integration” is slow since it divides the sample into discrete cells and evaluates corresponding ray paths. The “Harmonic coefficient” method is much faster and uses a simple approximation.

From the point of view of the user interface the two methods provide a similar panel and parameters. The only difference is that in “Harmonic integration” there is an additional field to control the number of divisions for the integration path and we just describe the “Harmonic coefficient” one. The model uses the same description of sample shape as the Popa model (Popa, 1998) to describe the anisotropic crystallite size. In analogy to that method, the user needs to choose the Laue group for the sample shape symmetry and the maximum harmonic expansion term (L_{\max}). L_{\max} should be the minimum number that permits to describe sufficiently the absorption by the sample. We point out that especially for the “Harmonic coefficient” model, due to the approximations used, the goal is not to get the real shape of the sample but the best correction for the absorption. Shape may not correspond to the real one. Other options are needed to provide sufficient flexibility for the model to work in different conditions. Sample orientation angles permit to rotate the coordinate system for the absorption correction. This way the symmetry of sample shape/absorption can be decoupled from the texture sample symmetries. The velocity absorption correction should be enabled for TOF experiments. The last two

parameters are the model weight and the standard size. The first controls the weight between absorption in reflection and in transmission.

The model in its approximation considers two different paths inside the sample. The first path connects the center of the sample with the two points intersecting the incident and diffracted beams with the sample surface (only a line passing through the center is considered for computing speed reasons). The second path connects directly these two points. In reflection the first path is long and the second is short. In transmission both are long. Weighting between the two paths permits to refine a balance between transmission or reflection modes. We have found that a good starting value is 0.3 and the parameter should be refined only towards the end of the refinement if necessary. The last parameter (Standard size) is just a commodity value to speed up convergence. We have found that changing the overall size of the sample shape changes the overall intensity of the diffraction a lot, much more than any other parameter. In practice this prevents an effective refinement of the sample dimension and shape or the change in their parameters is very slow. The "Standard size" parameter normalizes the sample dimension by its value. So the program can change more quickly the sample shape coefficients counterbalancing the change in shape dimension by refining also this size normalization value to keep the same overall intensity. Therefore, this standard size parameter should be refined along with the harmonic coefficients. Absorption pole figures can be plotted from the texture plot window. This absorption model has been used in the past efficiently in cases of irregular shapes (Artioli *et al.*, 2003; Xie *et al.*, 2004; Volz *et al.*, 2006).

(h) For *multiphase materials*, the contribution of individual phases to the diffraction pattern in the "Plot" representation can be evaluated by right clicking on the phase label in the plot. It will show different phases with different colors.

(i) *Magnetic scattering*. At present only a simple "cone model" (Hastings and Corliss, 1962) is implemented. One of the advantages of neutrons is that they are sensitive to magnetic scattering and can be used to determine magnetic pole figures (Birsan *et al.*, 1996; Brockhouse, 1953; Bunge, 1989).

VII. CONCLUSION

Quantitative texture analysis is of critical importance to evaluate deformation processes both of man-made as well as natural materials. It is also the basis for determining anisotropic physical properties of polycrystalline aggregates. Since crystallite orientation affects diffraction intensities, consideration of texture is also crucial for evaluating volume fractions and for crystal structure refinements of materials that have preferred orientation. The Rietveld texture analysis of HIPPO-TOF neutron diffraction data with MAUD has been applied to a wide range of samples such as metals (e.g., Matthies *et al.*, 2005), ceramics (e.g., Jones *et al.*, 2005), as well as rocks (e.g., Pehl and Wenk, 2005), including high-temperature conditions inside a furnace (e.g., Bhattacharyya *et al.*, 2006; Lonardelli *et al.*, 2007; Wenk *et al.*, 2009). These procedures will, no doubt, be further refined, and we hope that this brief introduction will make texture analysis

more palatable for uninitiated HIPPO users, as well as users of other TOF neutron diffractometers. HIPPO is available through the LANSCE user program, see <http://www.lansce.lanl.gov>. Remember the four steps: (1) load the HIPPO data with the HIPPO Wizard, (2) enter phase (or phases), and (3) refine with the Analysis Wizard (Texture), (4) export the orientation distribution in E-WIMV, and calculate pole figures in BEARTEX. A sample without major complexities is finished in 1 to 2 h on an average PC.

ACKNOWLEDGMENTS

Part of this procedure was developed for the Third HIPPO in December 2006 at U.C. Berkeley, supported by the UCOP-CLC program to foster Campus Laboratory collaboration. It has since then been greatly expanded based on valuable input from many users. Support was also obtained from NSF (Grant No. EAR 0836402), DOE (Grant No. DE-FG02-05ER15637), and CDAC. This work has benefited from the use of the Lujan Neutron Scattering Center at LANSCE, which is funded by the Office of Basic Energy Sciences, U.S. Department of Energy. Los Alamos National Laboratory is operated by Los Alamos National Security LLC under DOE Contract No. DE-AC52-06NA25396. We appreciate help from Pamela Kaercher and Adrian Losko.

- Artioli, G., Dugnani, M., Hansen, T., Lutterotti, L., Pedrotti, A., and Sperl, G. (2003). "Crystallographic texture analysis of the Iceman and coeval copper axes by non-invasive neutron powder diffraction," in *Die Gletschermumie aus der Kupferzeit 2*, edited by A. Fleckinger (Folio Verlag, Wien, Bozen), pp. 9–22.
- Bhattacharyya, D., Viswanathan, G. B., Vogel, S. C., Williams, D. J., Venkatesh, V., and Fraser, H. L. (2006). "A study of the mechanism of α to β phase transformation by tracking texture evolution with temperature in Ti-6Al-4V using neutron diffraction," *Scr. Mater.* **54**, 231–236.
- Birsan, M., Szpunar, J. A., Tun, Z., and Root, J. H. (1996). "Magnetic texture determination using nonpolarized neutron diffraction," *Phys. Rev. B* **53**, 6412–6417.
- Brockhouse, B. N. (1953). "The initial magnetization of nickel under tension," *Can. J. Phys.* **31**, 339–355.
- Brown, D. W., Bourke, M. A. M., Field, R. D., Hulth, W. L., Teter, D. F., Thoma, D. J., and Vogel, S. C. (2006). "Neutron diffraction study of the deformation mechanisms of the uranium-7% niobium shape memory alloy," *Mater. Sci. Eng., A* **421**, 15–21.
- Bunge, H. J. (1965). "Zur Darstellung allgemeiner Texturen," *Z. Metallkd.* **56**, 872–874.
- Bunge, H.-J. (1982). *Texture Analysis in Materials Science—Mathematical Methods* (Butterworths, London).
- Bunge, H. J. (1989). "Texture and magnetic properties," *Textures Microstruct.* **11**, 75–91.
- Caglioti, G., Paoletti, A., and Ricci, F. P. (1958). "Choice of collimators for a crystal spectrometer for neutron diffraction," *Nucl. Instrum.* **3**, 223–228.
- Caglioti, G., Paoletti, A., and Ricci, F. P. (1960). "On resolution and luminosity of a neutron diffraction spectrometer for single crystal analysis," *Nucl. Instrum. Methods* **9**, 195–198.
- Day, P., Enderby, J. E., Williams, W. G., Chapon, L. C., Hannon, A. C., Radaelli, P. G., and Soper, A. K. (2004). "GEM: The general materials diffractometer at ISIS—Multibank capabilities for studying crystalline and disordered materials," *Neutron News* **15**, 19–23.
- Dollase, W. A. (1986). "Correction of intensities for preferred orientation in powder diffractometry: Application of the March model," *J. Appl. Crystallogr.* **19**, 267–272.
- Downs, R. T. and Wallace-Hall, M. (2003). "The American Mineralogist crystal structure database," *Am. Mineral.* **88**, 247–250.
- Grazulis, S., Chateigner, D., Downs, R. T., Yokochi, A. F. T., Quiros, M., Lutterotti, L., Manakova, E., Butkus, J., Moock, P., and Le Bail, A. (2009). "Crystallography open database—An open access collection of crystal structures," *J. Appl. Crystallogr.* **42**, 726–729.

- Hartig, C., Vogel, S. C., and Mecking, H. (2006). "In-situ measurement of texture and elastic strains with HIPPO-CRATES," *Mater. Sci. Eng., A* **437**, 145–150.
- Hastings, J. M. and Corliss, L. M. (1962). "Magnetic structure of manganese chromite," *Phys. Rev.* **126**, 556–565.
- Ivankina, T. I., Kern, H., and Nikitin, A. N. (2005). "Directional dependence of P - and S -wave propagation and polarization in foliated rocks from the Kola superdeep well: Evidence from laboratory measurements and calculations based on TOF neutron diffraction," *Tectonophysics* **407**, 25–42.
- Izumi, F. and Momma, K. (2007). "Three-dimensional visualization in powder diffraction," *Diffus. Defect Data, Pt. B* **130**, 15–20.
- Jones, J. L., Hoffman, M., and Vogel, S. C. (2007). "Ferroelastic domain switching in lead zirconate titanate measured by *in situ* neutron diffraction," *Mechanics of Materials* **39**, 283–290.
- Kocks, U. F., Tomé, C. N., and Wenk, H.-R. (2000). *Texture and Anisotropy: Preferred Orientations in Polycrystals and their Effect on Materials Properties*, 2nd ed. (Cambridge University Press, Cambridge).
- Larson, A. C. and Von Dreele, R. B. (2004). General Structure Analysis System (GSAS), Report LAUR 86-748, Los Alamos National Laboratory, Los Alamos, N.M.
- LeBail, A., Duroy, H., and Fourquet, J. L. (1988). "Ab-initio structure determination of LiSbWO_6 by X-ray powder diffraction," *Mater. Res. Bull.* **23**, 447–452.
- Lonardelli, I., Gey, N., Wenk, H.-R., Humbert, M., Vogel, S. C., and Lutterotti, L. (2007). "In situ observation of texture evolution during α - β and β - α phase transformations in titanium alloys investigated by neutron diffraction," *Acta Mater.* **55**, 5718–5727.
- Lonardelli, I., Wenk, H.-R., Lutterotti, L., and Goodwin, M. (2005). "Texture analysis from synchrotron diffraction images with the Rietveld method: Dinosaur tendon and salmon scale," *J. Synchrotron Radiat.* **12**, 354–360.
- Lutterotti, L. and Bortolotti, M. (2005). "Algorithms for solving crystal structures using texture," *Acta Crystallogr., Sect. A: Found. Crystallogr.* **61**, c158–c159.
- Lutterotti, L., Ceccato, R., Dal Maschio, R., and Pagani, E. (1998). "Quantitative analysis of silicate glass in ceramic materials by the Rietveld method," *Mater. Sci. Forum* **278–281**, 87–92.
- Lutterotti, L., Chateigner, D., Ferrari, S., and Ricote, J. (2004). "Texture, residual stress and structural analysis of thin films using a combined X-ray analysis," *Thin Solid Films* **450**, 34–41.
- Lutterotti, L., Matthies, S., Wenk, H.-R., Schultz, A. J., and Richardson, J. W. (1997). "Combined texture and structure analysis of deformed limestone from time-of-flight neutron diffraction spectra," *J. Appl. Phys.* **81**, 594–600.
- Lutterotti, L. and Scardi, P. (1992). "Profile fitting by the interference function," *Adv. X-Ray Anal.* **35A**, 577–584.
- Lutterotti, L. and Scardi, P. (1990). "Simultaneous structure and size-strain refinement by the Rietveld method," *J. Appl. Crystallogr.* **23**, 246–252.
- Lutterotti, L., Voltolini, M., Wenk, H.-R., Bandyopadhyay, K., and Vanorio, T. (2010). "Texture analysis of turbostratically disordered Camontmorillonite," *Am. Mineral.* **95**, 98–103.
- Matthies, S., Lutterotti, L., and Wenk, H.-R. (1997). "Advances in texture analysis from diffraction spectra," *J. Appl. Crystallogr.* **30**, 31–42.
- Matthies, S., Pehl, J., Wenk, H.-R., and Vogel, S. (2005). "Quantitative texture analysis with the HIPPO TOF diffractometer," *J. Appl. Crystallogr.* **38**, 462–475.
- Matthies, S. and Vinel, G. W. (1982). "On the reproduction of the orientation distribution function of textured samples from reduced pole figures using the concept of conditional ghost correction," *Phys. Status Solidi B* **112**, K111–K114.
- Matthies, S. and Wagner, F. (1996). "On a $1/n$ law in texture related single orientation analysis," *Phys. Status Solidi B* **196**, K11–K15.
- McDaniel, S., Bennett, K., Durham, W. B., and Waddington, E. D. (2006). "In situ deformation apparatus for time-of-flight neutron diffraction: Texture development of polycrystalline ice I_h ," *Rev. Sci. Instrum.* **77**, 093902(1-6).
- Pehl, J. and Wenk, H.-R. (2005). "Evidence for regional Dauphiné twinning in quartz from the Santa Rosa mylonite zone in Southern California. A neutron diffraction study," *J. Struct. Geol.* **27**, 1741–1749.
- Popa, N. C. (1998). "The hkl dependence of diffraction-line broadening caused by strain and size for all Laue groups in Rietveld refinement," *J. Appl. Crystallogr.* **31**, 176–180.
- Popa, N. C. and Balzar, D. (2002). "An analytical approximation for the size-broadened profile given by the lognormal and gamma distributions," *J. Appl. Crystallogr.* **35**, 338–346.
- Reiche, H. M. and Vogel, S. C. (2010). "A versatile automated sample changer for texture measurements on the HIPPO neutron diffractometer," *Rev. Sci. Instrum.* **81**.
- Rietveld, H. M. (1969). "A profile refinement method for nuclear and magnetic structures," *J. Appl. Crystallogr.* **2**, 65–71.
- Rodríguez-Carvajal, J. (1993). "Recent advances in magnetic structure determination by neutron powder diffraction," *Physica B* **192**, 55–69.
- Roe, R. J. (1965). "Description of crystalline orientation in polycrystalline materials III, general solution to pole figure inversion," *J. Appl. Phys.* **36**, 2024–2031.
- Sonneveld, E. J. and Visser, J. W. (1975). "Automatic collection of powder data from photographs," *J. Appl. Crystallogr.* **8**, 1–7.
- Toby, B. H. (2006). "R factors in Rietveld analysis: How good is good enough?" *Powder Diffr.* **21**, 67–70.
- Ullemeyer, K., Spalthoff, P., Heinitz, J., Isakov, N. N., Nikitin, A. N., and Weber, K. (1998). "The SKAT texture diffractometer at the pulsed reactor IBR-2 at Dubna: Experimental layout and first measurements," *Nucl. Instrum. Methods Phys. Res. A* **412**, 80–88.
- Vogel, S. C., Hartig, C., Lutterotti, L., Von Dreele, R. B., Wenk, H.-R., and Williams, D. J. (2004). "Texture measurements using the new neutron diffractometer HIPPO and their analysis using the Rietveld method," *Powder Diffr.* **19**, 65–68.
- Volz, H. M., Vogel, S. C., Necker, C. T., Roberts, J. A., Lawson, A. C., Williams, D. J., Daemen, L. L., Lutterotti, L., and Pehl, J. (2006). "Rietveld texture analysis by neutron diffraction of highly absorbing materials," *Powder Diffr.* **21**, 114–117.
- Von Dreele, R. B. (1997). "Quantitative texture analysis by Rietveld refinement," *J. Appl. Crystallogr.* **30**, 517–525.
- Wenk, H.-R. (2006). "Neutron diffraction texture analysis," *Rev. Mineral. Geochem.* **63**, 399–426.
- Wenk, H.-R. (2011). "Texture analysis by advanced diffraction methods," in *Modern Diffraction Methods*, edited by E. Mittemeyer and U. Welzel (in press), Chap. 8.
- Wenk, H.-R., Barton, N., Bortolotti, M., Vogel, S. C., Voltolini, M., Lloyd, G., and Gonzalez, G. (2009). "Dauphiné twinning and texture memory in polycrystalline quartz. Part 3. Texture memory during phase transformations," *Phys. Chem. Minerals* **37**, 567–583.
- Wenk, H.-R., Cont, L., Xie, Y., Lutterotti, L., Ratschbacher, L., and Richardson, J. (2001). "Rietveld texture analysis of Dabie Shan eclogite from TOF neutron diffraction spectra," *J. Appl. Crystallogr.* **34**, 442–453.
- Wenk, H.-R., Huensche, I., and Kestens, L. (2007). "In situ observation of texture changes in ultralow carbon steel," *Mater. Trans.* **30**, 261–267.
- Wenk, H. R. and Kocks, U. F. (1987). "The representation of orientation distributions," *Metall. Trans. A* **18A**, 1083–1092.
- Wenk, H.-R., Lonardelli, I., Rybacki, E., Dresen, G., Barton, N., Franz, H., and Gonzalez, G. (2006). "Dauphiné twinning and texture memory in polycrystalline quartz. Part 1: Experimental deformation of novaculite," *Phys. Chem. Miner.* **33**, 667–676.
- Wenk, H.-R., Lutterotti, L., and Vogel, S. (2003). "Texture analysis with the new HIPPO TOF diffractometer," *Nucl. Instrum. Methods Phys. Res. A* **515**, 575–588.
- Wenk, H.-R., Matthies, S., Donovan, J., and Chateigner, D. (1998). "BEARTEX, a Windows-based program system for quantitative texture analysis," *J. Appl. Crystallogr.* **31**, 262–269.
- Xie, Y., Wenk, H.-R., Lutterotti, L., and Kovacs, F. (2004). "Texture analysis of ancient coins with TOF neutron diffraction," *J. Mater. Sci.* **39**, 3329–3337.
- Xie, Y., Wenk, H.-R., and Matthies, S. (2003). "Plagioclase preferred orientation by TOF neutron diffraction and SEM-EBSD," *Tectonophysics* **370**, 269–286.